AGU PUBLICATIONS

JGR

Journal of Geophysical Research: Space Physics

RESEARCH ARTICLE
10.1002/2015JA021497

Key Points:
- A vertical shear in zonal drifts of ESF 3 m irregularities is detected at low latitude
- The shear centers at an apex altitude of 650 km over dip equator
- Better knowledge of plasma zonal drift shear at low latitude are needed

Correspondence to:
G. Li,
gzlee@mail.iggcas.ac.cn

Citation:
Li, G., B. Ning, L. Liu, M. A. Abdu, W. Wan, and L. Hu (2015), Shear in the zonal drifts of 3 m irregularities inside spread *F* plumes observed over Sanya, *J. Geophys. Res. Space Physics*, *120*, 8146–8154, doi:10.1002/2015JA021497.

Received 27 MAY 2015
Accepted 29 AUG 2015
Accepted article online 3 SEP 2015
Published online 29 SEP 2015

Shear in the zonal drifts of 3 m irregularities inside spread *F* plumes observed over Sanya

Guozhu Li[1,2], Baiqi Ning[1,3], Libo Liu[1], M. A. Abdu[4], Weixing Wan[1], and Lianhuan Hu[1]

[1]Key Laboratory of Earth and Planetary Physics, Institute of Geology and Geophysics, Chinese Academy of Sciences, Beijing, China, [2]Beijing National Observatory of Space Environment, Institute of Geology and Geophysics, Chinese Academy of Sciences, Beijing, China, [3]State Key Laboratory of Space Weather, Chinese Academy of Sciences, Beijing, China, [4]Divisão de Aeronomia, Instituto Nacional de Pesquisas Espaciais, São Paulo, Brazil

Abstract Incoherent scatter radars near magnetic equator regularly measured a vertical shear in zonal drifts of the evening background plasma, with westward drifts below the equatorial *F* region peak and eastward drifts above. We report here observations of a clear shear structure in the zonal drifts of 3 m irregularities inside spread *F* (SF) backscatter plumes measured with a 47.5 MHz coherent scatter radar operated at a low-latitude site Sanya (18.4°N, 109.6°E; dip latitude 12.8°N). The radar interferometry analysis on the zonal drifts of the 3 m irregularities yields results consistent with that estimated from the irregularity echo Doppler velocity measurements with multiple beams. It is shown that the SF 3 m irregularities move westward at the lowest altitudes, while at higher altitudes in the same SF plume structure, the 3 m irregularities drift eastward. One interesting point is that the vertical shear of zonal drifts was centered at ~300 km altitude over Sanya, which maps to an apex altitude of ~650 km at magnetic equator and is thus apparently higher than the apex altitudes 250–450 km where the zonal velocity shear has usually been observed. Analysis of the observations suggests that while the possibility of local generation of the shear flow of the irregularities can exist, the possibility of a plasma vortex appearing at relative high altitudes causing the zonal drift shear of *F* region 3 m irregularities measured over Sanya cannot be totally ruled out.

1. Introduction

The zonal drifts of equatorial spread *F* (ESF) irregularities have been widely studied using spatially separated ionospheric scintillation receivers, all-sky airglow imager, and VHF radar with multibeam steering or interferometry capability [e.g., *Kudeki et al.*, 1981; *Abdu et al.*, 1987; *Bhattacharyya et al.*, 2002; *Martinis et al.*, 2003; *Yokoyama et al.*, 2004; *Otsuka et al.*, 2006; *Muella et al.*, 2008; *Li et al.*, 2012a; *Patra et al.*, 2015]. These studies showed that under geomagnetic quiet conditions, the zonal drifts of ESF irregularities are, mostly, eastward and decrease as a function of time with a few notable exceptions. The eastward drift velocity of the irregularities and its variation with local time are similar to those of the background *F* region plasma drifts obtained from incoherent scatter radar and satellite in situ observations [*Fejer et al.*, 2013]. It was suggested that the eastward drifts are due to the downward electric field predominating in the nighttime equatorial *F* region, driving the eastward plasma motions through $\mathbf{E} \times \mathbf{B}$ force. By tracking 630 nm nightglow depletions, some researchers measured the ESF/plasma bubble drifts and found that the eastward drifts of plasma bubbles reverse and turn westward near midnight [e.g., *Taylor et al.*, 1997; *Abdu et al.*, 2003]. They suggested that the westward drifts could be caused by disturbance dynamo effect of enhanced geomagnetic activity. However, *Bhattacharyya et al.* [2002] deduced the zonal drifts of smaller-scale irregularities from two spaced scintillation receivers along a magnetic E-W baseline over Ancon; westward drifts associated with freshly generated ESF irregularities during geomagnetic quiet conditions were found. The initially observed westward drifts were seen to decrease with local time and turn into eastward at ~20:30 LT that lasted till later in the night.

There are several possibilities which may cause the westward drifts of ESF irregularities at a specific altitude/time, such as that the *F* region downward electric field (due to *F* region dynamo) could reverse itself and turns upward, the low-latitude *E* region dynamo could take over and cause upward electric field at equatorial *F* region, and the polarization electric field generated inside a tilted ESF bubble structure could have a strong upward component [e.g., *Kudeki et al.*, 1981; *Taylor et al.*, 1997; *Huang et al.*, 2010]. Using the Jicamarca radar interferometer measurements, *Kudeki et al.* [1981] reported that the zonal drifts of equatorial

F region 3 m irregularities during evening hours showed a strong shear, with westward velocities below ~450 km altitude and eastward above. *Tsunoda et al.* [1981] pointed out that the zonal drift shear, together with the preceding upward motion of plasma due to the prereversal enhancement of eastward electric field, would form a vortex-like structure in the height-time velocity map. Later improved incoherent and coherent scatter radar observations over Jicamarca showed a clear snapshot of the evening background plasma vortex and identified that the shear in zonal drifts of 3 m irregularities was directly associated with the equatorial *F* region background plasma vortex [*Kudeki and Bhattacharyya*, 1999]. The vortex was found to center below the main *F* layer, about 250 km altitude, and be elongated in horizontal direction with a dimension of a few thousand kilometers at solar minimum. More recently, *Lee et al.* [2015] investigated the morphology of plasma vortex by using the Jicamarca radar observations at solar maximum. They reported that besides the sunset background plasma vortex regularly measured at ~270 km altitude, another smaller vortex might appear about 0.5–1 h later at higher altitudes. All the observed plasma vortexes were centered below the apex altitude of ~450 km over magnetic equator. According to these observations, the zonal drifts of ESF irregularities during postsunset, toward the east or west, would be closely associated with the tilt of the ESF plume/bubble, the altitude and/or latitude where the irregularities are observed, and the altitude where the plasma vortex is located.

Previous experimental studies of the shear in zonal drifts associated with plasma vortex were mostly performed using equatorial incoherent/coherent scatter radars at two longitudes, i.e., Jicamarca and Kwajalein. Besides the experimental observations, *Rodrigues et al.* [2012] simulated the evening background plasma vortex by employing the Thermosphere-Ionosphere-Electrodynamics General Circulation Model (TIEGCM). Their simulation results reproduced the plasma vortex structure similar to that obtained from the Jicamarca radar and revealed that the shear in zonal drifts could occur at all longitudes. Importantly, the simulation results showed that the altitude of the zonal drift shear was unlikely to depend on the solar activity but varied with longitude; the shear altitude was centered at ~275, 300, and 375 km in the longitudes of 230°E, 120°E, and 10°E, respectively. In this regard, more recent numerical simulations using the TIEGCM coupled with the Global Ionosphere-Plasmasphere (GIP) model showed that the plasma vortex, however, could extend to higher altitudes of more than 1000 km [*Richmond et al*., 2015].

In this paper, we present an unusual case of spread *F* (SF) backscatter plume detected by the Sanya (18.4°N, 109.6°E; dip latitude 12.8°N) VHF coherent radar on 27 September 2012 (geomagnetic quiet day). The zonal drift velocities of 3 m irregularities inside the spread *F* backscatter plume reverse from westward below ~300 km altitude to eastward above. It is worth pointing out that the shear in zonal drifts of *F* region irregularities observed at low latitude, where the magnetic field lines map to higher apex altitudes above the magnetic equator, has not been previously reported. This observational result raises challenging questions on nature of the low-latitude zonal drift shear and its possible connection with high-apex-altitude plasma vortex.

2. Data Processing

The Sanya VHF radar, operating at 47.5 MHz with a peak power of 24 kW, is sensitive to 3 m irregularities and has been used to investigate the low-latitude ionosphere and meteor trail irregularities over China since its installation in February 2009 [e.g., *Li et al*., 2012a, 2012b]. During September 2012, the Sanya radar was operated with a five-beam steering mode to investigate the occurrence characteristics of spread *F* backscatter plumes. The five beams, positioned at directions from west to east, with azimuth and zenith angles of (315°, 33°), (328°, 29°), (0°, 23°), (32°, 29°), and (45°, 33°), respectively, satisfy the geomagnetic field line perpendicularity conditions in the ionospheric *E* and *F* regions due to the relatively wider beam width (10° × 24°). A detailed description of the radar parameters for the five-beam steering experiment has been given by *Li et al.* [2012a]. Figure 1 shows that for the radar beam oriented at ~23° zenith angle, an altitude of 300 km over Sanya can be mapped to an apex altitude of ~650 km over dip equator by using the International Geomagnetic Reference Field model (IGRF-2010). For the spread *F* backscatter plume observations presented here, the signal-to-noise ratio (SNR) and the mean Doppler velocity were computed online using the moment method [e.g., *Woodman*, 1985; *Ning et al*., 2012]. The received complex echo signals, i.e., the raw I/Q components, were recorded for off-line interferometry analysis.

To investigate the zonal drifts of 3 m irregularities inside an ESF backscatter plume, the Doppler velocity measured by the multiple beams pointed in east and west directions [e.g., *Patra et al*., 2015] and the radar interferometry technique [e.g., *Kudeki et al*., 1981] was employed in this paper. On the basis of the Doppler

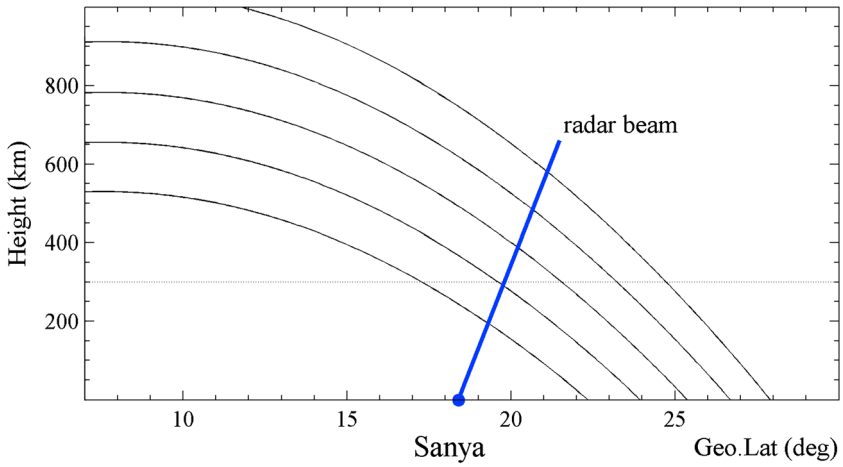

Figure 1. Magnetic field geometry showing how different altitude regions over Sanya are connected to apex altitudes over dip equator through the conducting magnetic field lines.

velocities (V_d) observed by the east or west beams of the Sanya radar, the zonal drifts of irregularities (V) were estimated according to $V = V_d/\sin\alpha$, where α is the azimuth angle of the beam direction. On the other hand, by using the phase difference (φ) of SF irregularity echoes between any two receiving channels aligned in the magnetic east-west direction, we calculated the zonal drifts also according to the time rate of the echoing region displacement (δx). This zonal drift calculation is similar to that we did in our earlier interferometry analysis of meteor trail irregularities in which we used the westernmost and easternmost channels of the Sanya radar antenna array [e.g., *Li et al.*, 2012b].

3. Results

Figure 2 shows the backscatter plume event observed on 27 September 2012. Earlier multiple instrument observations have proved that the towering irregularity plumes shown in radar height-time-intensity (HTI) maps, such as the backscatter plume structures presented in Figures 2a–2e, represent the ESF plumes produced by the equatorial plasma bubbles (EPBs) [e.g., *Tsunoda and White*, 1981]. In the simultaneous C/NOFS satellite in situ density measurements, several plasma density depletions were identified during 12:00–14:00 UT on 27 September around the Sanya longitude (figure not shown here). This indicates that the spread *F* backscatter plume event shown in Figure 2 is indeed associated with ESF/EPB development. The 3 h *Kp* indices on 27 September were 3−, 2−, 1+, 1−, 0+, 0+, 0+, and 1. The backscatter echo intensity and the Doppler velocity profiles are shown in the left and right plots, respectively. The echo height is calculated using the IGRF-2010 and by considering perpendicularity between the radar beam and the magnetic field in different range bins. The black dotted curve in Figure 2i shows the variation of *F* layer peak height (h_mF_2) obtained from the co-located Digisonde over Sanya. The red vertical axis on the left of each plot represents the apex altitude over the magnetic equator. The black and red slant lines show the height displacement of the local and apex sunset terminators over Sanya and magnetic equator, respectively.

As seen in Figures 2a–2e, the ESF backscatter plume first appeared in the westernmost beam around 13:00 UT (2018 LT, LT = UT + 7.3) with durations of about 40 min and was sequentially detected by other beams to the east. This indicates that the initial occurrence of the plume should be located to the west of the westernmost beam. The bulk of the ESF plume drifted eastward into and out of the radar field of view. This is a regular feature for postsunset ESF backscatter plumes observed over low latitude. For example, using the equatorial atmosphere radar (EAR) and Sanya VHF radar multibeam steering measurements, *Li et al.* [2013] reported that the periodic plume structures measured by the two radars, as a group, drifted eastward during postsunset hours. The line-of-sight Doppler velocities measured by west (east) beams of the Sanya VHF radar, although were not shown in their paper, were mostly negative (positive), indicating that the bulk motion of irregularities inside ESF plumes was also eastward. However, for the Doppler velocity measurements shown in Figures 2f–2j (for example around ~13:10 UT as indicated by the vertical dashed line marked with "I"), the velocity patterns of the ESF irregularities obtained from the west beams 4 and 5 (Figures 2i and 2j), with

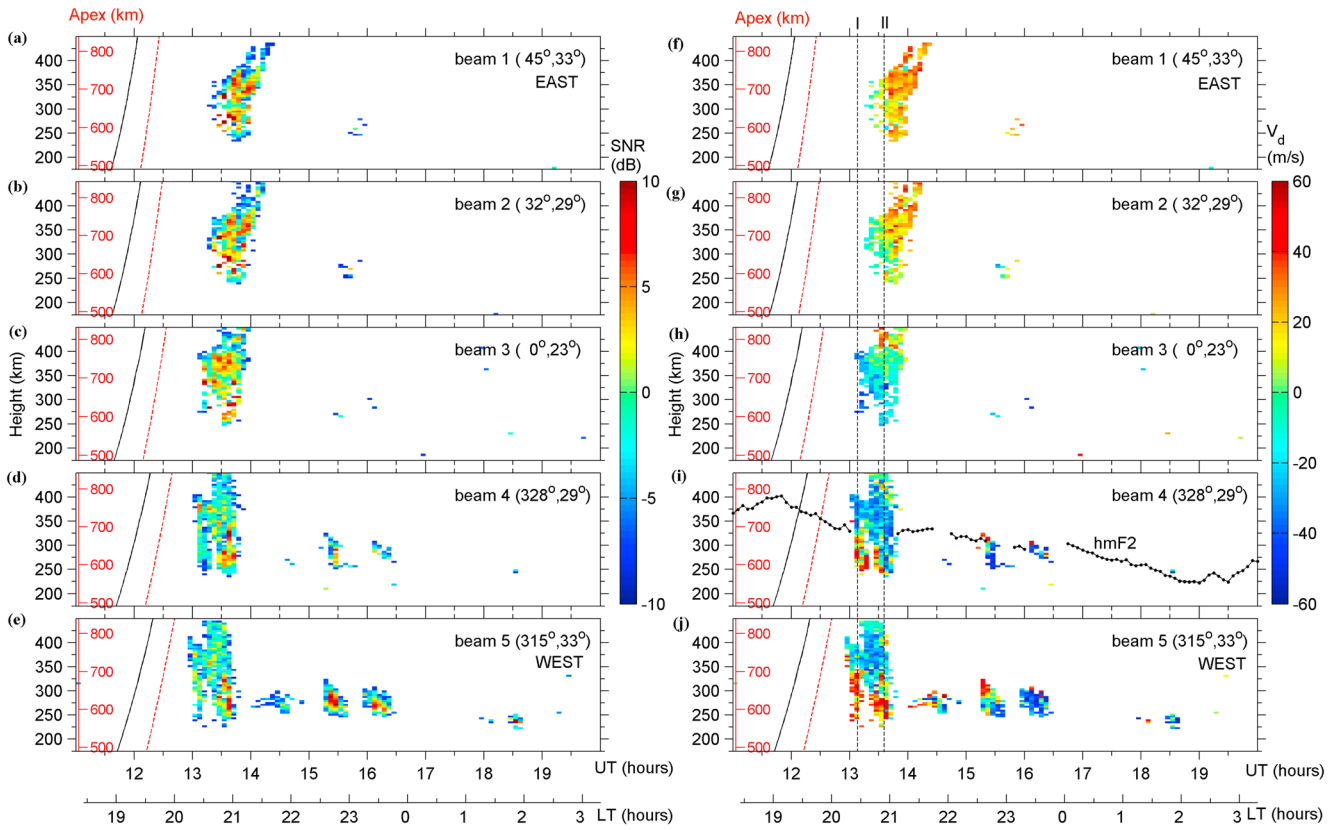

Figure 2. (a–e) Height-time-intensity (HTI) plots of backscatter plume echoes observed with the Sanya VHF radar during 11:00–20:00 UT on 27 September 2012. (f–j) Height-time Doppler velocity plots of the backscatter plume echoes. Positive (negative) velocity represents irregularity motion away from (toward) the radar. The black dotted curve in Figure 2i shows the variation of *F* layer peak height (h_mF_2). The red vertical axis in each panel indicates the apex altitude over dip equator. The black and red slant lines show the local and apex sunset terminators, respectively.

positive and negative values at lower and higher altitudes, respectively, are significantly different from those reported earlier over Sanya. The predominantly positive and negative Doppler velocities at lower and higher altitudes represent irregularities motion away from and toward the radar, respectively.

For the east (or west) tilted beam, the Doppler velocity measured along the beam direction is a combination of the zonal and vertical velocity components of irregularity drifts. While considering the ESF plume case shown in Figure 2, if the observed Doppler velocity shear mainly results from the component of vertical velocity, it would mean the ESF plume irregularities at lower and higher altitudes motion upward and downward, respectively. This, however, may not be true since earlier numerical model simulations and experimental observations both showed that the irregularities generally move upward during the initial phase of ESF plume development or the irregularities at lower and higher altitudes move downward and upward, respectively, due to the bubble detaching process during later phase of plume development [e.g., *Sahai et al.*, 2006]. Further, it can be seen from the northward/upward beam measurements (Figure 2h) that the Doppler velocities at lower and higher altitudes are negative and positive, representing irregularities move downward and upward, respectively. According to the observations and earlier simulations, the Doppler velocity shear of ESF plume irregularity measured by the west beams 4 and 5 (Figures 2i and 2j) should be mainly related to a shear in zonal drifts rather than in vertical drifts. A vertical shear in zonal drifts of irregularities, with westward and eastward velocities at lower and higher altitudes, respectively, appeared at the west of Sanya and produced the Doppler velocity pattern seen in the west beams. Specifically, the collocated ionosonde measurements show that the shear was centered near the *F* layer peak height (as indicated by the black solid curve in Figure 2i). On the other hand, the Doppler velocities obtained from the east beams 1 and 2 after ~13:35 UT (20:53 LT, as indicated by the vertical dotted line marked with "II") are mostly positive with relatively larger values compared to that of the northward beam, indicating that the irregularities at both higher and lower

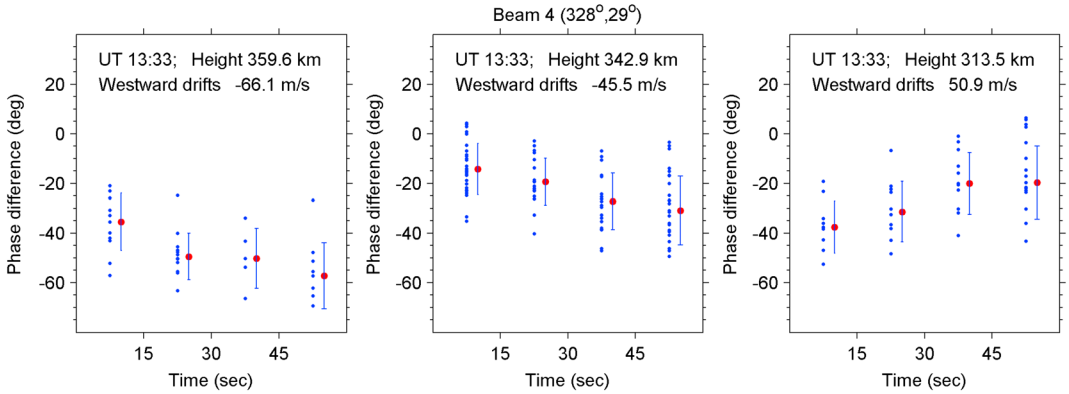

Figure 3. The phase angles derived from interferometry analysis of ESF plume irregularity echoes. A decrease in the mean phase difference (red dot) corresponds to a displacement of the echoing region to the east.

altitudes drift eastward in the east of Sanya. Thus, we note that during the period of this measurements, the zonal drift was generally eastward at all higher heights, while at lower heights (beam 4) it was westward in the beginning and became eastward later.

Besides the Doppler velocity measurements, the phase differences between the westernmost and easternmost receiving channels of the Sanya radar antenna array can be used to estimate the zonal drifts of irregularities with the radar interferometry technique [e.g., *Kudeki et al.*, 1981; *Li et al.*, 2012b]. Note that due to low-coherence values associated with weak echoes, only a few echoes with SNR $>$ 5 dB could be utilized to derive the zonal drifts of irregularities. As an example, Figure 3 shows the phase differences at several range bins for the west beam 4 (328°, 29°). The blue dots represent the phase differences. The mean phase difference (φ) at each time interval is shown as a red dot and shifted rightward 2.5 s for clarity. A decrease in the mean phase difference corresponds to a displacement of the echoing region to the east. It is clear from the figure that the irregularities at higher (342.9 km and 359.6 km) and lower (313.5 km) altitudes move eastward and westward, respectively. In a similar way as was done by *Li et al.* [2012b], we calculated the zonal drift velocity. As shown in the top of each plot, the estimated zonal drift velocities at altitudes 359.6, 342.9, and 313.5 km are -66.1, -45.5, and 50.9 m/s, respectively (negative means eastward). Although only limited interferometry measurements can be obtained (due to low SNR), the results shown in Figure 3 provide additional support to the zonal drifts determined from Doppler velocity measurements.

Figure 4 shows the zonal drift velocity (V) profile variation with time determined from the Doppler velocities (V_d) of the west beams 4 and 5. It is relevant to mention that in many studies of E region irregularity, the zonal drifts have been derived from the Doppler velocities of east (V_{de}) and west (V_{dw}) beams using the expression $V = (V_{de} - V_{dw})/2\sin\alpha$ to eliminate the effect of irregularity vertical drift [e.g., *Patra et al.*, 2015]. This method, however, is based on the assumption that the irregularities seen in the east and west beams drift with the

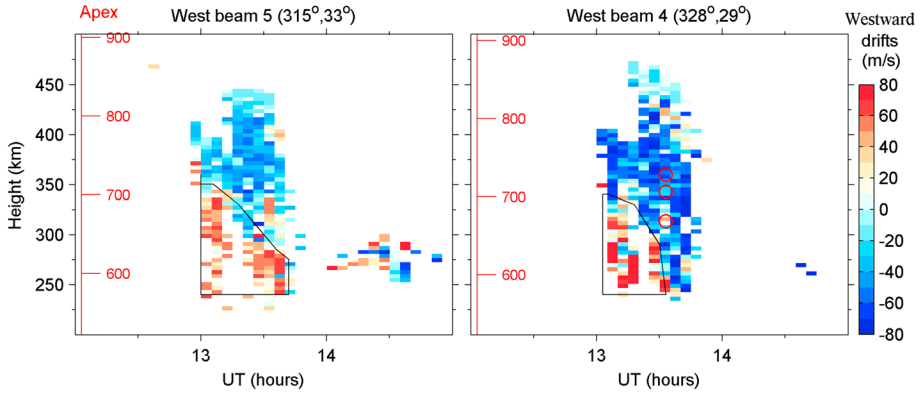

Figure 4. The zonal drift velocity profiles estimated with the Doppler velocity measurements of ESF plume irregularity echoes.

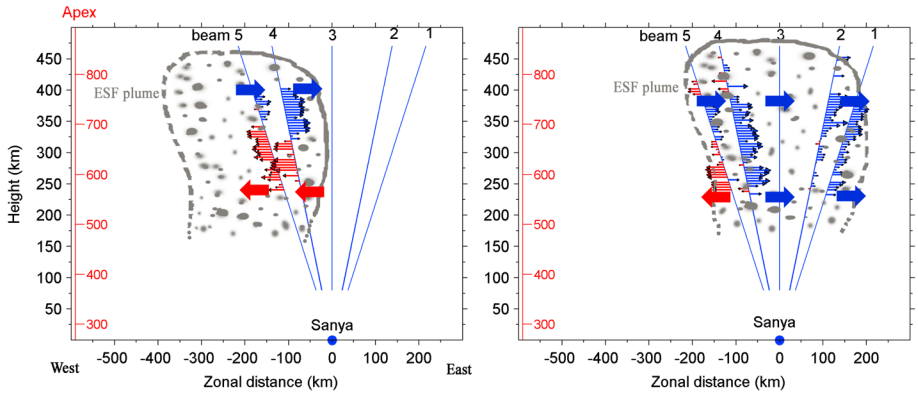

Figure 5. Schematic diagram representing the spatial and temporal variations of the vertical shear in zonal drifts of ESF plume irregularities detected at two time intervals, (left) ~13:10 UT and (right) 13:35 UT.

same zonal/vertical velocity. Using the radar imaging technique, *Hysell and Woodman* [1997] reported that the Doppler velocities of irregularities located within the *F* region density depletion structure are apparently higher than those of irregularities located along the boundary of the depletion. For the present ESF irregularity case, the height-time Doppler velocity maps of the different beams (Figure 2) show that the drift patterns in east and west beams are obviously different; a Doppler velocity shear is seen in west beams but not in east beams. Thus, we calculated the zonal drifts of irregularities, separately according to $V = V_d/\sin\alpha$ for each beam. Note that the drifts calculated with the Doppler shifts could represent the phase velocity of irregularities. On the other hand, using this expression, the numerical values of the zonal drifts could be contaminated by the vertical drifts. But as mentioned in the previous paragraph, the direction of irregularity motion, toward east or west, can be determined. Also, the red circles in the right plot of Figure 4 indicate the time and altitude where the radar interferometer technique is employed to calculate the zonal drifts shown in Figure 3. It shows that the zonal drifts calculated with the Doppler velocities are similar to those obtained from the radar interferometry observations. In general, Figure 4 shows that a vertical shear in zonal drifts of ESF irregularities appeared around 250–350 km during 13:00–13:45 UT (20:18–21:03 LT). The higher and lower altitude velocities are eastward and westward, with an average value of −24 m/s and 23 m/s, respectively.

4. Discussion

The observation by the Sanya VHF radar on 27 September 2012 shows that a vertical shear in zonal drifts of postsunset ESF 3 m irregularities is unambiguously detected in the west beams. By examining all the multibeam steering observations of spread *F* irregularities with the Sanya radar (a total of about 7 months), we found that several other cases could also have possible shear structures, but they are not as clear as the case shown in Figure 2. Using the ion drift velocities obtained from satellite in situ measurements, *Huang et al.* [2010] reported the presence of eastward and westward drifts for irregularities inside the ESF bubbles/depletions. They suggested that the polarization electric field inside the tilted ESF bubbles could be stronger than the background electric field and thus control the motion of irregularities; the upward (downward) electric field corresponding to the west (east) tilted bubble structure causes a westward (eastward) drift. For the ESF irregularity observations by the Sanya VHF radar, Figure 5 shows a schematic representing the spatial and temporal variations of zonal drift shear. The left and right plots show the zonal drift measurements at two time intervals, ~13:10 UT and 13:35 UT, as marked with two vertical dashed lines (I and II) in Figure 2, respectively. For the higher-altitude irregularities inside the ESF plume, observations from both west and east beams show eastward drifts that are caused by downward electric field generally created by the *F* region dynamo. This is consistent with earlier studies of low-latitude ESF irregularities. As regards the lower-altitude westward drift, if that is driven by the polarization electric field generated inside a tilted ESF bubble, the plume/bubble structure at lower altitude should be strongly tilted to the west. This will cause similar westward drifts at lower altitudes for the east and west beams since the irregularities detected by these beams come from the same ESF plume. However, the westward drift is not seen in the east beams.

And as time progressed, the westward drift by the west beam 4 reversed and turned eastward at ~13:35 UT, whereas the zonal drift by beam 5 still remained westward at lower altitudes. Thus, the westward drifts of irregularities in our observation could not be induced by the tilt of ESF plume.

On the other hand, supporting evidence on the association between irregularity zonal drift shear and evening background plasma vortex was provided by *Kudeki et al.* [1981]; a zonal drift shear of 3 m irregularities with westward drifts below ~450 km and eastward drifts above was suggested to be linked with the evening background plasma vortex. Using numerical model simulations, *Rodrigues et al.* [2012] and *Richmond et al.* [2015] explained the vertical shear in plasma zonal drifts as being controlled by the neutral wind dynamo in the *F* region. The westward drifts associated with the evening background plasma vortex were suggested to be driven by the Pedersen conductivity-averaged westward winds and the polarization electric field due to the Cowling effect of the eastward electric field. Importantly, the simulations of *Richmond et al.* [2015] identified that the evening background plasma vortex can extend up to much greater apex altitudes (more than 1000 km) due to the effect of wind at low latitude up to nearly 30°. In the light of the simulation results of evening background plasma vortex, we may argue that the zonal drift shear of ESF irregularities can perhaps be linked with an evening background plasma vortex centered at a relative higher apex altitude of ~650 km. This, however, needs to be testified in the future since there is still no direct observational evidence on the high-altitude evening background plasma vortex.

Besides the regularly observed evening background plasma vortex which is centered around 300 km over dip equator, more recent studies have shown that there is another smaller vortex that appeared at a higher altitude around 450 km [*Kil et al.*, 2014; *Lee et al.*, 2015]. Using a total of 30 days of Jicamarca incoherent scatter radar data at solar maximum, Lee et al. investigated the statistical occurrence characteristic of plasma vortex during postsunset hours. It was found that the shear altitude of the smaller vortex did not represent the center of the evening background plasma vortex but always stayed inside the ESF. Kil et al. suggested that the westward motion of irregularities inside ESF plumes/bubbles could resemble the motion of irregularities that appeared in the bottom-type spread *F* where the plumes/bubbles originate and evening background plasma vortex exists. Although the bottom-type spread *F* is not detected in our observation due to the fact that the field lines at equatorial *F* region bottomside map to the *E* layer over Sanya, we can expect the conditions for a bottom-type spread *F* layer to exist preceding the irregularities at the base of the ESF plume over dip equator. On the other hand, *Rodrigues et al.* [2012] pointed out that the small, secondary vortex could be caused by the development of ionospheric irregularities. Since the shear in zonal drifts of ESF irregularities detected by the Sanya radar was centered at an altitude that corresponded to apex altitude of 650 km which is apparently higher than the altitude (~300 km) where the evening background plasma vortex regularly occurred, the zonal drift shear in our ESF observation seems more likely to be associated with the smaller vortex other than the evening background plasma vortex that has been suggested to be related to the origin of ESF.

The vortex pattern and the associated shear flow of the background plasma, as well as the shear in the zonal velocities of the backscatter irregularities discussed in the literature, are mainly confined to the dip equatorial region. Their direct applicability to the observations over Sanya, a low-latitude site, should involve some further inherent considerations. The eastward drifts of 3 m irregularities above ~300 km, observed in all the beams of Sanya radar, are consistent with the plasma zonal drifts in the background vortex flow as per the TIEGCM-GIP simulation by *Richmond et al.* [2015] for solar medium and higher activity conditions. These zonal plasma drifts are, in large part, representative of the field line-integrated Pedersen conductivity-weighted zonal wind that extends to low latitudes. The model result by Richmond et al., however, does not predict a westward background plasma flow over a low-latitude site such as Sanya. The zonal wind, and hence the plasma flow, below about 300 km shown in their simulations turns eastward over the equator as well as over low latitudes after about 20:30 LT. On the other hand, if the vertical electric fields inside the backscatter plume irregularities (of a few meter-scale size) were to drive the westward drift, even relative to a background plasma that may be drifting eastward, then such electric field will not map to the equatorial apex height of their field lines. Thus, two possibilities to be considered are (1) if the westward drift of ESF 3 m irregularities observed (as part of the vertical shear) over Sanya till ~21:00 LT is part of a background plasma vortex, in which case the polarization electric field inside the irregularities should be weak, making themselves tracers of the background plasma motion, or (2) if the irregularity zonal drift is driven by the polarization electric field of the irregularities which is significantly more intense than the background vertical electric field that drives the ambient plasma. Based on the simulation results by Richmond et al., the first possibility appears highly unlikely, since the ambient plasma vortex center (near 300 km) maps to the *E* region over Sanya. The second

possibility deserves serious consideration based on the following reasoning: the meter-scale irregularities constituting the plume structure are believed to be produced by secondary cascading instability processes that operate at the steep density gradient regions at the walls of large-scale bubble structures; the density gradient can be stronger at low latitudes where the background electron density is higher (as per the 3-D simulation by *Keskinen et al*. [2003]). In other words, local conditions dictate the irregularity growth so that their electric fields, which do not map to the field line apex heights, could be responsible for their westward drift. Such electric field can be weaker at a later phase of the bubble growth that could also explain the drift reversal from west to east at lower altitudes. Also, the situation of the zonal drift of the irregularities inside ESF plumes resembling the westward motion of the bottom-type spread *F* irregularities, as suggested by *Kil et al.* [2014], may be a coexisting possibility.

5. Conclusion

We presented a case study of vertical shear in zonal drifts of ESF irregularities made using the Sanya VHF coherent backscatter radar at low latitude. The observations clearly showed that the shear structure appeared in the west beams of the Sanya radar and varied with time. The shear was centered at 300 km which corresponded to an equatorial apex altitude of ~650 km that is apparently too high for the observed shear to be associated with a vortex structure of the evening equatorial ionosphere. Even though there has been suggestion of an extremely high-altitude plasma vortex, we cannot ascertain from the present data set whether our observation can belong to such a background plasma vortex or to smaller vortex associated with plasma disturbance in ESF. The explanations we have provided here are only tentative ones. In any case, more experimental works from other low-latitude radars with fast beam steering capability, for example, the EAR over Kototabang and the newly installed VHF radar over Gadanki, will be helpful for understanding the morphology of vertical shear in zonal drifts of low-latitude ESF irregularities. The Doppler velocity measurements in the radar-wide field of view with sufficiently temporal and spatial resolution could provide more detailed information on the shear structure evolution. Further, we anticipate that the correlative studies of evening background plasma vortex and zonal drift shear of ESF irregularities at low latitude in Southeast Asia will be conducted in the future using incoherent scatter radar (ISR) over Sanya. The construction of the Sanya ISR (with a peak power of ~2 MW) is underway and will be completed in 2018.

Acknowledgments
The data used in this paper can be obtained on request from G.Z. (gzlee@mail.iggcas.ac.cn) and L.H. (hulh@mail.iggcas.ac.cn). This research is supported by the National Natural Science Foundation of China (41422404, 41174136, 41374163, and 41374164), the Open Research Program of State Key Laboratory of Space Weather, Chinese Academy of Sciences, and the National Important Basic Research Project of China (2012CB825604).

Alan Rodger thanks the reviewers for their assistance in evaluating this paper.

References

Abdu, M. A., J. H. A. Sobral, Y. Nakamura, and C. J. Zamlutti (1987), Equatorial plasma bubble zonal velocity height gradient from spaced VHF polarimeter and scanning 630-nm measurements, *Geophys. Res. Lett.*, *14*, 965–968, doi:10.1029/GL014i009p00965.

Abdu, M. A., I. S. Batista, H. Takahashi, J. MacDougall, J. H. Sobral, A. F. Medeiros, and N. B. Trivedi (2003), Magnetospheric disturbance induced equatorial plasma bubble development and dynamics: A case study in Brazilian sector, *J. Geophys. Res.*, *108*(A12), 1449, doi:10.1029/2002JA009721.

Bhattacharyya, A., S. Basu, K. M. Groves, C. E. Valladares, and R. Sheehan (2002), Effect of magnetic activity on the dynamics of equatorial *F* region irregularities, *J. Geophys. Res.*, *107*(A12), 1489, doi:10.1029/2002JA009644.

Fejer, B. G., B. D. Tracy, and R. F. Pfaff (2013), Equatorial zonal plasma drifts measured by the C/NOFS satellite during the 2008–2011 solar minimum, *J. Geophys. Res. Space Physics*, *118*, 3891–3897, doi:10.1002/jgra.50382.

Huang, C.-S., O. de La Beaujardiere, R. F. Pfaff, J. M. Retterer, P. A. Roddy, D. E. Hunton, Y.-J. Su, S.-Y. Su, and F. J. Rich (2010), Zonal drift of plasma particles inside equatorial plasma bubbles and its relation to the zonal drift of the bubble structure, *J. Geophys. Res.*, *115*, A07316, doi:10.1029/2010JA015324.

Hysell, D. L., and R. F. Woodman (1997), Imaging coherent backscatter radar observations of topside equatorial spread *F*, *Radio Sci.*, *32*(6), 2309–2320, doi:10.1029/97RS01802.

Keskinen, M. J., S. L. Ossakow, and B. G. Fejer (2003), Three dimensional nonlinear evolution of equatorial spread-*F* bubbles, *Geophys. Res. Lett.*, *30*(16), 1855, doi:10.1029/2003GL017418.

Kil, H., W. K. Lee, Y.-S. Kwak, Y. Zhang, L. J. Paxton, and M. Milla (2014), The zonal motion of equatorial plasma bubbles relative to the background ionosphere, *J. Geophys. Res. Space Physics*, *119*, 5943–5950, doi:10.1002/2014JA019963.

Kudeki, E., and S. Bhattacharyya (1999), Postsunset vortex in equatorial *F*-region plasma drifts and implications for bottomside spread-*F*, *J. Geophys. Res.*, *104*(A12), 28,163–28,170, doi:10.1029/1998JA900111.

Kudeki, E., B. G. Fejer, D. T. Farley, and H. M. Ierkic (1981), Interferometer studies of equatorial *F* region irregularities and drifts, *Geophys. Res. Lett.*, *8*(4), 377–380, doi:10.1029/GL008i004p00377.

Lee, W. K., H. Kil, Y.-S. Kwak, and L. J. Paxton (2015), Morphology of the postsunset vortex in the equatorial ionospheric plasma drift, *Geophys. Res. Lett.*, *42*, 9–14, doi:10.1002/2014GL062019.

Li, G., B. Ning, M. A. Abdu, W. Wan, and L. Hu (2012a), Precursor signatures and evolution of post-sunset equatorial spread-*F* observed over Sanya, *J. Geophys. Res.*, *117*, A08321, doi:10.1029/2012JA017820.

Li, G., B. Ning, L. Hu, Y.-H. Chu, I. M. Reid, and B. K. Dolman (2012b), A comparison of lower thermospheric winds derived from range spread and specular meteor trail echoes, *J. Geophys. Res.*, *117*, A03310, doi:10.1029/2011JA016847.

Li, G., B. Ning, M. A. Abdu, Y. Otsuka, T. Yokoyama, M. Yamamoto, and L. Liu (2013), Longitudinal characteristics of spread *F* backscatter plumes observed with the EAR and Sanya VHF radar in Southeast Asia, *J. Geophys. Res. Space Physics*, *118*, 6544–6557, doi:10.1002/jgra.50581.

Martinis, C., J. V. Eccles, J. Baumgardner, J. Manzano, and M. Mendillo (2003), Latitude dependence of zonal plasma drifts obtained from dual-site airglow observations, *J. Geophys. Res.*, *108*(A3), 1129, doi:10.1029/2002JA009462.

Muella, M. T. A. H., E. R. de Paula, I. J. Kantor, I. S. Batista, J. H. A. Sobral, M. A. Abdu, P. M. Kintner, K. M. Groves, and P. F. Smorigo (2008), GPS L-band scintillations and ionospheric irregularity zonal drifts inferred at equatorial and low-latitude regions, *J. Atmos. Sol. Terr. Phys.*, *70*(10), 1261–1272, doi:10.1016/j.jastp.2008.03.013.

Ning, B., L. Hu, G. Li, L. Liu, and W. Wan (2012), The first time observations of low-latitude ionospheric irregularities by VHF radar in Hainan, *Sci. China Tech. Sci.*, doi:10.1007/s11431-012-4800-2.

Otsuka, Y., K. Shiokawa, and T. Ogawa (2006), Equatorial ionospheric scintillations and zonal irregularity drifts observed with closely-spaced GPS receivers in Indonesia, *J. Meteorol. Soc. Jpn.*, *84A*, 343–351.

Patra, A. K., P. Srinivasulu, P. P. Chaitanya, M. D. Rao, and A. Jayaraman (2015), First results on low-latitude *E* and *F* region irregularities obtained using the Gadanki Ionospheric Radar Interferometer, *J. Geophys. Res. Space Physics*, *119*, 10,276–10,293, doi:10.1002/2014JA020604.

Richmond, A. D., T.-W. Fang, and A. Maute (2015), Electrodynamics of the equatorial evening ionosphere: 1. Importance of winds in different regions, *J. Geophys. Res. Space Physics*, *120*, 2118–2132, doi:10.1002/2014JA020934.

Rodrigues, F. S., G. Crowley, R. A. Heelis, A. Maute, and A. Reynolds (2012), On TIE-GCM simulation of the evening equatorial plasma vortex, *J. Geophys. Res.*, *117*, A05307, doi:10.1029/2011JA017369.

Sahai, Y., J. R. Abalde, P. R. Fagundes, V. G. Pillat, and J. A. Bittencourt (2006), First observations of detached equatorial ionospheric plasma depletions using OI 630.0 nm and OI 777.4 nm emissions nightglow imaging, *Geophys. Res. Lett.*, *33*, L11104, doi:10.1029/2005GL025262.

Taylor, M. J., J. V. Eccles, J. LaBelle, and J. H. A. Sobral (1997), High resolution OI (630 nm) image measurements of *F*-region depletion drifts during the Guará campaign, *Geophys. Res. Lett.*, *24*, 1699–1702, doi:10.1029/97GL01207.

Tsunoda, R. T., and B. R. White (1981), On the generation and growth of equatorial backscatter plumes 1. Wave structure in the bottomside *F* layer, *J. Geophys. Res.*, *86*(A5), 3610–3616, doi:10.1029/JA086iA05p03610.

Tsunoda, R. T., R. C. Livingston, and C. L. Rino (1981), Evidence of a velocity shear in bulk plasma motion associated with the post-sunset rise of the equatorial *F*-layer, *Geophys. Res. Lett.*, *8*, 807–810, doi:10.1029/GL008i007p00807.

Woodman, R. F. (1985), Spectral moment estimation in MST radars, *Radio Sci.*, *20*(6), 1185–1195, doi:10.1029/RS020i006p01185.

Yokoyama, T., S. Fukao, and M. Yamamoto (2004), Relationship of the onset of equatorial *F*-region irregularities with the sunset terminator observed with the equatorial atmosphere radar, *Geophys. Res. Lett.*, *31*, L24804, doi:10.1029/2004GL021529.